Reducing turbulent transport in toroidal configurations *via* shaping

H.E. Mynick[1], N.Pomphrey[1], and P. Xanthopoulos[2]

[1]*Plasma Physics Laboratory, Princeton University, Princeton, NJ*

[2]*Max-Planck-Institut für Plasmaphysik, Teilinstitut Greifswald, Greifswald, Germany*

Recent progress in reducing turbulent transport in stellarators and tokamaks by 3D shaping using a stellarator optimization code in conjunction with a gyrokinetic code is presented. The original applications of the method focussed on ion temperature gradient transport in a quasi-axisymmetric stellarator design. Here, an examination of both other turbulence channels and other starting configurations is initiated. It is found that the designs evolved for transport from ion temperature gradient turbulence also display reduced transport from other transport channels whose modes are also stabilized by improved curvature, such as electron temperature gradient and ballooning modes. The optimizer is also applied to evolving from a tokamak, finding appreciable turbulence reduction for these devices as well. From these studies, improved understanding is obtained of why the deformations found by the optimizer are beneficial, and these deformations are related to earlier theoretical work in both stellarators and tokamaks.

PACS #s: 52.55.Hc, 52.65.Tt, 52.35.Ra

I. INTRODUCTION

In recent work,[1] we have demonstrated a method by which stellarator designs with substantially reduced turbulent transport can be evolved from designs without this "turbulent optimization". Since turbulent transport is typically the dominant transport channel in today's neoclassical (NC) transport-optimized stellarator designs as well as in axisymmetric toroidal devices, such a capability has the potential to considerably improve the attractiveness of fusion *via* magnetic confinement.

The method makes use of two powerful numerical tools not available until recently, *viz.*, gyrokinetic (GK) codes valid for 3D nonlinear simulations, such as the GENE/GIST code

package[2,3], and stellarator optimization codes such as STELLOPT[4]. Because direct use of a performance figure of merit such as the radial heat flux Q_{GK} from GK simulations in the STELLOPT cost function would be too computationally expensive at present, we have developed "proxy functions" Q_{prox} to stand in for Q_{GK} in the STELLOPT runs, and then use GENE simulations to confirm the transport improvement. Our initial simulations and model for Q_{prox} have been for ion temperature gradient (ITG) turbulence with adiabatic electrons. As noted at the end of Ref. 1, the "proof-of principle" configurations described there represent the beginning of an exploration of the possibilities opened with this approach. In the present paper, we describe some of the progress we have made in this exploration.

II. κ_1–BOOSTING

The proxy function used in Ref. 1 is a quasilinear model for ITG turbulent transport, $Q_{prox} = Q_i = -\chi n_0 g^{rr} dT_i/dr$, with conductivity $\chi = \sum_{\mathbf{k}} D_{\mathbf{k}}$, $D_{\mathbf{k}} \simeq c_D \gamma_{\mathbf{k}}/k_r^2$, and growth rate $\gamma_{\mathbf{k}} \simeq (\omega_{*i}/\kappa_n)|\tau\kappa_1(\kappa_p - \kappa_{cr})|^{1/2} H(\kappa_p - \kappa_{cr}) H(-\kappa_1)$ coming from a simplified ITG dispersion equation. Here, $\kappa_1 \equiv \mathbf{e}_r \cdot \boldsymbol{\kappa}$ is the radial component of the vector curvature $\boldsymbol{\kappa}$, with $\mathbf{e}_r$ the covariant basis vector for minor radial coordinate $r \equiv (2\psi_t/B_a)^{1/2}$, $2\pi\psi_t$ the toroidal flux, B_a the magnetic field strength B at the plasma edge (where $r = a$), and $g^{rr} \equiv |\nabla r|^2$ the rr component of the metric tensor. Thus, κ_1 is negative for "bad" curvature, and positive for "good" curvature. $H(\kappa)$ is the Heavyside function, ω_{*i} is the diamagnetic frequency, and $\kappa_n \equiv L_n^{-1} \equiv -\partial_r \ln n_0$. The critical pressure gradient κ_{cr} and multiplicative constant c_D were determined by a best fit of Q_{prox} to the GK results for a set of flux tubes on a family of toroidal configurations studied earlier[5], with values 0.053 and 0.959, respectively.

We briefly recapitulate the results of Ref. 1. Starting with the LI383 baseline design for the quasi-axisymmetric (QA) National Compact Stellarator Experiment (NCSX)[6] at $\beta = 4.2\%$, STELLOPT evolved the configuration, constrained to retain the same plasma β, RB_t (= major radius × toroidal field) and aspect ratio. From two similar runs two configurations were evolved, called QA_35q and QA_40n. In Fig. 1 is shown the κ_1 profile along a field line for poloidal angle θ running from $-\pi$ to π for these 3 configurations, designated by black, green and red, respectively. As expected, the NCSX profile is tokamak-like, negative on the outboard side ($\theta \sim 0$), and positive toward the inboard side ($\theta \sim \pm\pi$). One notes that for the 2 evolved configurations STELLOPT has contrived to deform NCSX to "boost"

κ_1, substantially reducing the domain over which κ_1 is negative, as well as reducing $\gamma_{\mathbf{k}}$ in these domains, and thereby reducing Q_{prox}. As discussed in Ref. 1, the beneficial effect of this on turbulent transport was confirmed by nonlinear GENE runs, shown in Fig. 2, plotting the spatially-averaged heat fluxes for these devices versus time. These runs use $N_r \times N_y \times N_z = 64 \times 96 \times 128$ grid points in the r (radial), y (binormal), and z (parallel) directions, and $N_{v_\parallel} \times N_\mu = 32 \times 8$ points in velocity space, with $a\kappa_n \equiv -a\partial_r \ln n = 0, a\kappa_T \equiv -a\partial_r \ln T = 3, r_0/a \simeq 0.7, \tau \equiv T_e/T_i = 1$, and $L_r = L_y$, with $L_{r,y}$ the box size in the r and y directions, and $L_y/\rho_s = 2\pi/.05$. Time is in units of a/c_s, the heat flux Q is in units of $\rho_s^2 c_s p_{i0}/a^2$, with c_s the sound speed, $\rho_s \equiv c_s/\Omega_i$, Ω_i the ion gyrofrequency, and p_{i0} the unperturbed pressure. Fig. 2 shows a reduction below the NCSX level of a factor of about 2 for QA_40n, and 2.5 for QA_35q. While the reduction in turbulent transport in 35q is largely offset by an increase in NC transport, in 40n both the turbulent and NC transport levels were reduced from those of NCSX.

Not addressed in Ref. 1 is insight into the *means* by which the deformation found by STELLOPT achieved this κ_1-boosting. A first clue to this is provided by the profiles of rotational transform $\iota(s \equiv (r/a)^2)$ in Fig. 3. One notes that $\iota(s \to 0)$ becomes very small for QA_35q and QA_40n, while for NCSX it remains the dominant part of ι, $\iota_0 \equiv \iota(s = 0) \simeq 0.4$. Since $\iota \sim (r/a)^{2|m-2|}$ for a stellarator with a pure helical perturbation[7] with poloidal mode number $m = 2$, the large ι_0 value for NCSX indicates a large $m = 2$ contribution to its shape, while the small ι_0 values for the evolved configurations indicate a shape dominated by mode numbers $m \geq 3$. In 1965, Taylor[8] showed that a stellarator having $m \geq 3$ with an applied vertical field B_v of appropriate sign would have a magnetic well, $d^2V/d\psi_t^2 < 0$, where $V' \equiv dV/d\psi_t \equiv \int dl/B$. In vacuum, this criterion is equivalent to the "average curvature" criterion for interchange stability $\langle\kappa_1\rangle > 0$. Since the horizontal displacement Δ scales as $B_v/\iota(r)$, the rise of ι with increasing s for such a system displaces its inner flux surfaces more than its outer ones. With a correct choice of the sign of B_v, the surfaces are displaced outward, resulting in an enhanced poloidal field B_p on the outboard side, causing the field line to pass more rapidly through the bad-curvature region, as manifested for QA_35q and QA_40n in Fig. 1. In Fig. 4 are plotted the flux surfaces for NCSX at toroidal azimuth $\zeta = 0$ and π, and in Fig. 5 we plot the surfaces for QA_35q. The surfaces for QA_40n are similar. One sees appreciable outward displacement of the inner surfaces for QA_35q, versus little displacement for NCSX. Thus, in these evolved configurations, STELLOPT has boosted κ_1 by

removing much of the $m = 2$ shaping in NCSX, inducing the differential shift and improved $\langle \kappa_1 \rangle$ Taylor envisioned.

III. SHAPING TOKAMAKS

Since shaping *via* STELLOPT has had success for stellarator configurations, the question arises whether the same method could be used to reduce turbulent transport in tokamaks as well. Two general types of deformations may be considered, (a)those which preserve the device axisymmetry, and (b)nonaxisymmetric ones. In the latter case, other constraints can also be imposed which retain good NC transport, *e.g.*, *via* maintaining *quasi*-axisymmetry.

Figs. 6-8 show the result of applying axisymmetric perturbations, beginning with configuration TOK_52k (green), a device with shape approximating an axisymmetrized NCSX, but with tokamak-like current and ι profiles. Constraining the shape as before, again at $\beta = 4.2\%$, STELLOPT produces evolved configuration TOK_52q (red). Fig. 6 shows the poloidal cross-sections of these configurations. Also shown is the cross-section of NCSX (black) at $\zeta = \pi$. One notes that TOK_52q has acquired an indentation on the inboard side. As in Sec. II, the reason for the diminution of Q_{prox} is again due to boosting of κ_1, especially in the bad-curvature region, as one sees from the $\kappa_1(\theta)$ profiles in Fig. 7. In Fig. 8 is the corroborating comparison from GENE simulations. One notes that the large improvement in Q_{prox} in going from TOK_52k to TOK_52q is again mirrored by a large improvement in Q_{GK}, a factor of about 3. Such indentation is also known to be stabilizing for ballooning modes[12] and other MHD instabilities, again *via* improved average curvature. For both the QA and axisymmetric systems, the effect of the shape deformation which induces the improved average curvature has been to displace inner flux surfaces further out than the outer ones, an effect also induced by increasing the plasma β. Thus, one might expect that transport from ITG modes would also diminish with increasing β, an expectation borne out by initial tests with GENE.

Study of the effectiveness of *non*-axisymmetric perturbations (toroidal mode number $n \neq 0$) in reducing turbulent transport is at present just beginning. Because $\kappa_1 \simeq \partial_r B/B \sim |m|/a$, perturbations with larger m can can appreciably modify κ_1, even for modest shape deformations. Whether the size of $n \neq 0$ perturbations of an axisymmetric system needed to appreciably diminish Q is small enough that the modified system can still be regarded as

a tokamak rather than a stellarator remains to be seen.

IV. ETG TURBULENCE

Configurations QA_35q, QA_40n and TOK_52q were evolved to reduce ITG turbulent transport, but the issue of the transport due to other transport channels, such as from trapped-electron and electron temperature gradient (ETG)[10,11] turbulence, has not yet been addressed. ITG turbulence with adiabatic ions, as considered in our work thus far, addresses ion turbulent transport. Along with ITG transport with nonadiabatic electrons, these latter channels are expected to also be important for anomalous electron transport, which is less well understood and in many cases more problematic. Because of the close relationship between ITG and ETG instabilities, however, one might hope that shaping which reduces ITG transport could also reduce ETG transport. In Fig. 9 is shown some first corroboration of this, comparing $Q(t)$ for NCSX (black) and QA_40n (red), from GENE runs with kinetic electrons and adiabatic ions for the short wavelengths ($k_\theta \rho_e \lesssim 1$) of ETG turbulence. The runs use the same parameters as the ITG runs discussed earlier, but now with $L_{r,y}/\rho_s = 2\pi/3$. One sees that while the ETG turbulence is appreciable for NCSX, it appears almost completely stabilized for QA_40n. A comparison of GENE runs for ETG turbulence in the tokamaks TOK_52k and TOK_52q yields a similar large reduction in transport.

For both the ITG and ETG channels, the comparisons between transport in configurations noted so far have kept the profile gradients fixed. Another useful way to characterize the turbulence one might expect is the critical gradient κ_{Tcr}. A linear GENE study for this gives $a\kappa_{Tcr} = 1.49$ for NCSX, and 2.07 for QA_35q, consistent with improvement in the constant-gradient nonlinear results noted above.

V. DISCUSSION

In this paper, we have extended our use of the method described in Ref. 1 for reducing the levels of turbulent transport in toroidal devices of interest by refined shaping. For QA stellarator designs, the means by which STELLOPT achieved this by boosting the curvature κ_1 in going from NCSX to QA_35q or QA_40n has been found to be related to the outward-shift of flux surfaces first proposed by Taylor[8] for reasons of MHD stability. We have applied our

optimization method to tokamaks as well. In this case, STELLOPT has found a new instance of the earlier finding[12] that inboard indentation is beneficial for good average curvature in a tokamak, there resulting in stabilization of ballooning modes and easier access to a second-stability regime. Here, it has been found that the same kind of deformation supresses ITG turbulence as well. In addition to reducing ballooning and ITG turbulence, it has been demonstrated in these configurations that the κ_1-based proxy function used to reduce ITG turbulence also has a beneficial effect on ETG turbulence, possibly an even more important transport channel. [One notes that there may be deformations which boost κ_1 other than the ones (*e.g.*, inboard indentation) found thus far. These may be accessed by further constraining STELLOPT to prohibit the deformations it found most productive in reducing the cost function in the unconstrained runs.] For both the QA and axisymmetric systems to which the optimization method has been applied, the improved average curvature is achieved by deformations which displace inner flux surfaces outward more than the outer ones, similar to the effect of raising the plasma β, which initial explorations indicate also reduces the turbulence levels. Applying this optimization procedure to other interesting starting configurations, such as quasi-omnigenous and quasi-helical stellarators, is planned, as are improvements and extensions of the proxy function, including making greater use of other key geometric quantities found to significantly impact turbulence levels, such as the local shear, and possibly direct use of GENE in the optimization cycle.

Acknowledgment

The authors are grateful to A. Boozer, M. Chance, L.-P. Ku and M. Zarnstorff for valuable discussions. This work supported by U.S.Department of Energy Contract No.DE-AC02-09CH11466.

---

[1] H.E. Mynick, N. Pomphrey, P. Xanthopoulos, *Phys. Rev. Letters*, **105**, 095004 (2010).

[2] F. Jenko, W. Dorland, M. Kotschenreuther, B.N. Rogers, *Phys. Plasmas* **7**, 1904 (2000).

[3] P. Xanthopoulos, W.A. Cooper, F. Jenko, Yu. Turkin, A. Runov J. Geiger, *Phys. Plasmas* **16**, 082303 (2009).

[4] A. Reiman., G. Fu, S Hirshman, L. Ku, D. Monticello, H. Mynick, M. Redi, D. Spong, M. Zarnstorff, B. Blackwell, A. Boozer, A. Brooks, W.A. Cooper, M. Drevlak, R. Goldston, J. Harris, M. Isaev, C. Kessel, Z. Lin, J.F. Lyon, P. Merkel, M. Mikhailov, W. Miner, N. Nakajima, G. Neilson, C Nührenberg, M. Okamoto, N. Pomphrey, W. Reiersen, R. Sanchez, J. Schmidt, A. Subbotin, P. Valanju, K.Y. Watanabe, R White, *Plasma Phys. Control. Fusion* **41** B273 (1999).

[5] H.E. Mynick, P. Xanthopoulos and A.H. Boozer, *Phys.Plasmas* **16** 110702 (2009).

[6] G.H. Neilson, M.C. Zarnstorff, J.F. Lyon, the NCSX Team, *Journal of Plasma and Fusion Research* **78**, 214-219 (2002).

[7] K. Miyamoto, *Nucl.Fusion* **18** 243 (1978).

[8] J.B. Taylor, *Phys. Fluids* **8** 1203 (1965).

[9] J.P. Freidburg, *Ideal Magneto-Hydro-Dynamics*, (Plenum Press, New York, 1987), see p.373ff.

[10] F. Romanelli, *Physics of Fluids B* **1**, 1018 (1989).

[11] F. Jenko, W. Dorland, Phys. Rev. Lett. **89**, 225001 (2002).

[12] M.S. Chance, S.C. Jardin, T.H. Stix, *Phys. Rev. Letters* **51** 1963 (1983).

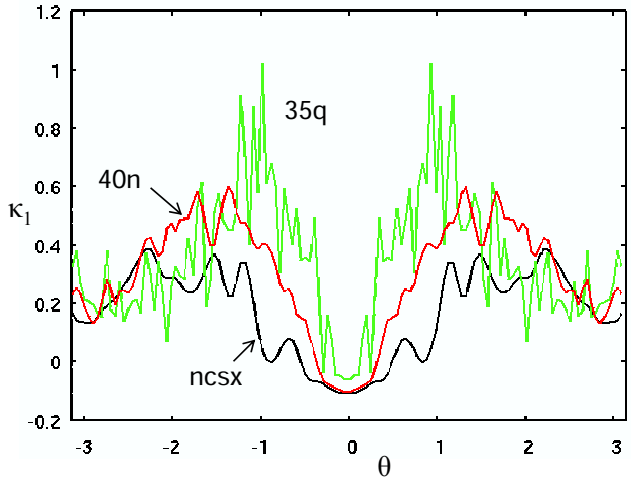

FIG. 1: (Color online) Comparison of radial curvature $\kappa_1(\theta)$ for 1 poloidal transit for NCSX (black), QA_35q (green) and QA_40n (red).

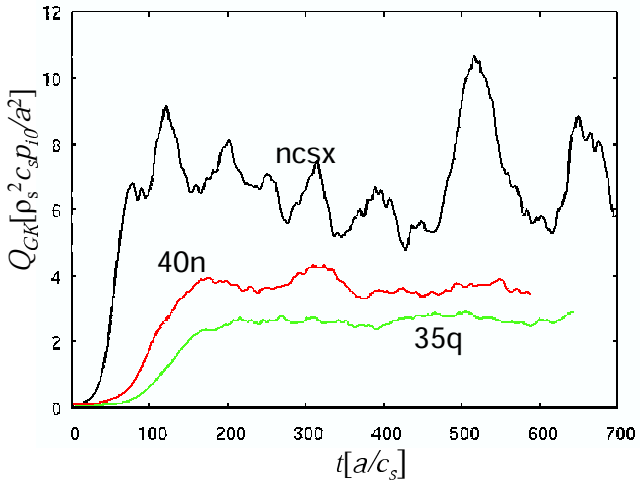

FIG. 2: (Color online) Comparison of line-averaged heat flux Q_{GK} versus time for NCSX (black), QA_35q (green), and QA_40n (red) from nonlinear GENE runs. QA_35q and QA_40n achieve reductions in turbulent transport over that in NCSX by factors of about 2.5 and 2, resp.

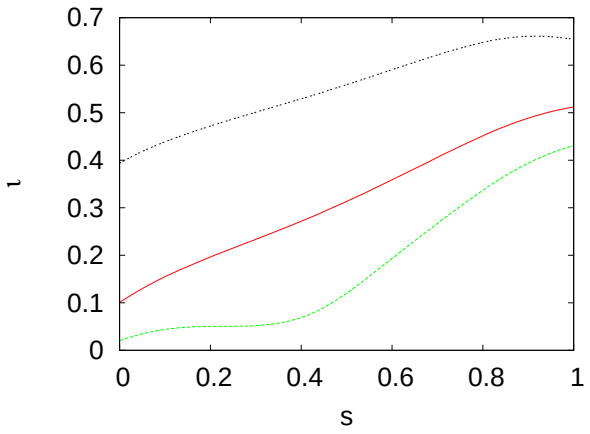

FIG. 3: (Color online) Profiles of rotational transform ι versus $s \equiv (x/a)^2$) for the same 3 configurations as in Figs. 1 and 2.

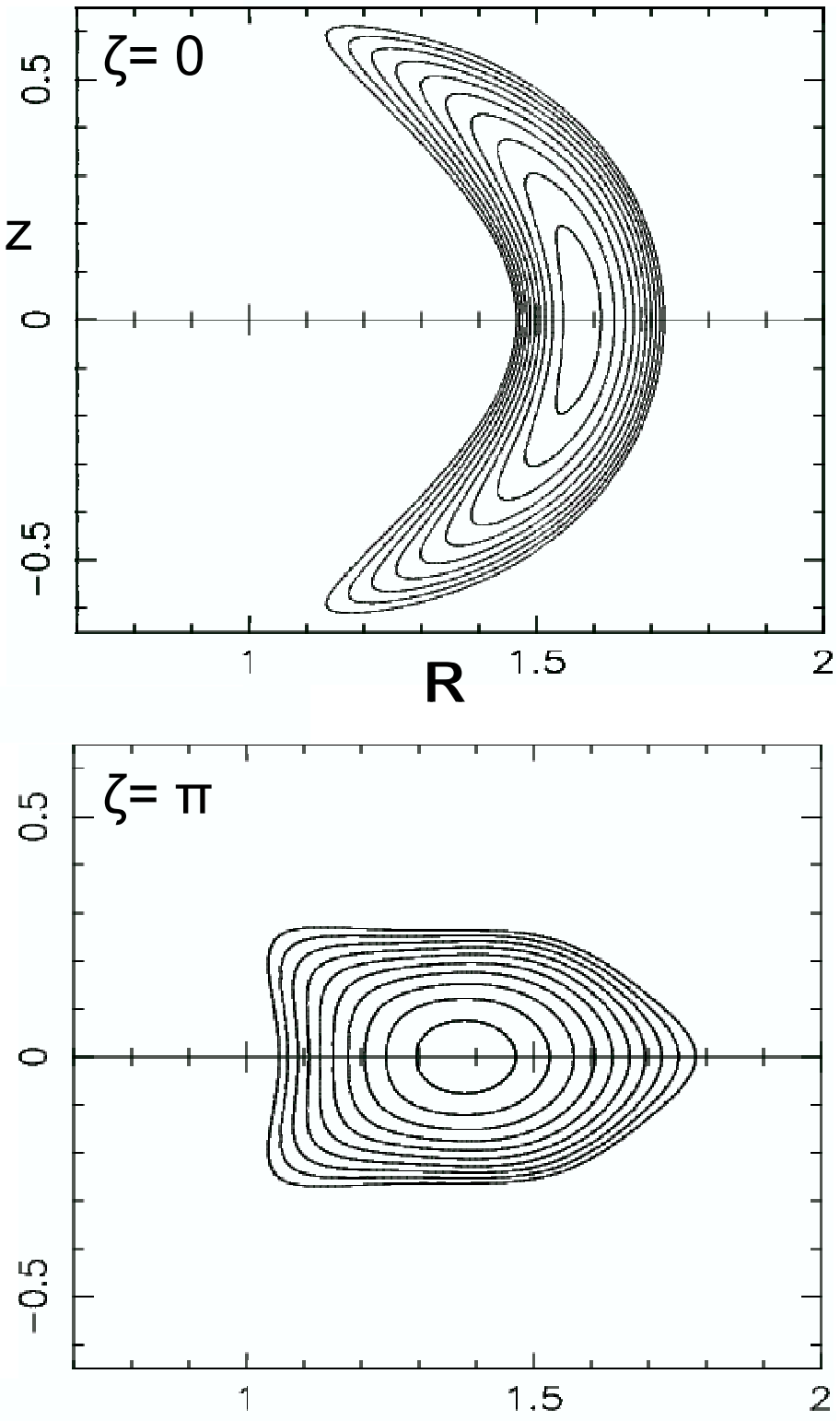

FIG. 4: (Color online) Flux surfaces of NCSX at $\zeta = 0$ and π.

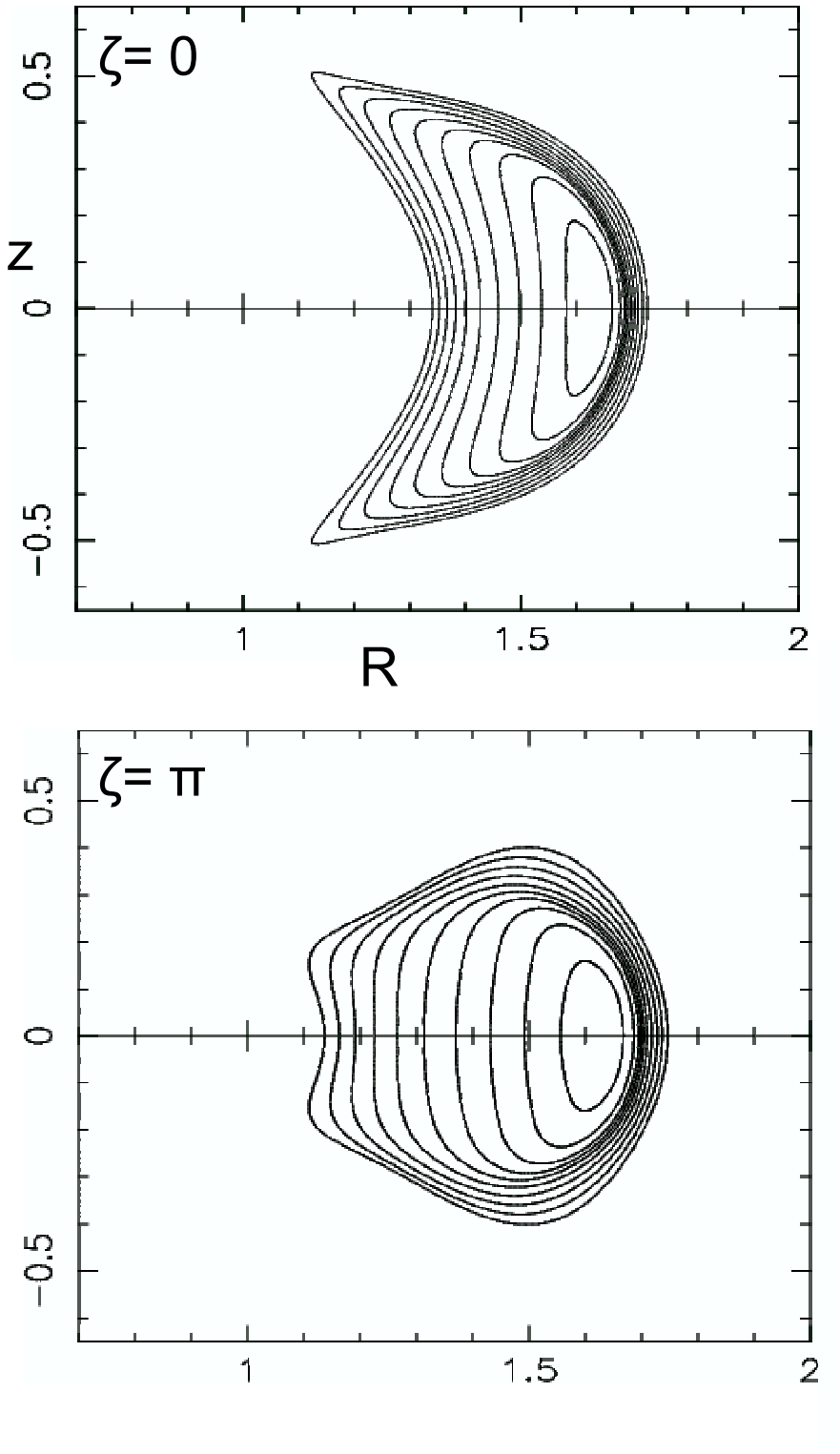

FIG. 5: (Color online) Flux surfaces of QA_35q at $\zeta = 0$ and π.

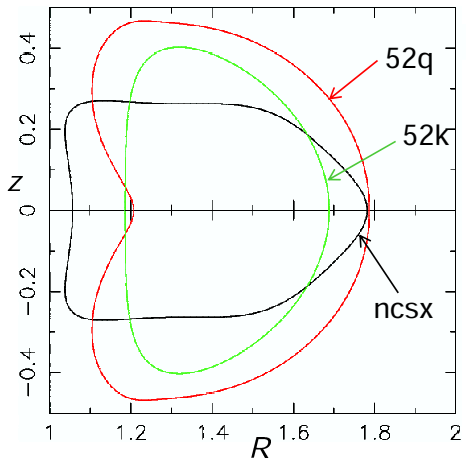

FIG. 6: (Color online) Poloidal cross sections of starting configuration TOK_52k (green), evolved configuration TOK_52q (red), and the stellarator NCSX at $\zeta = \pi$ (black).

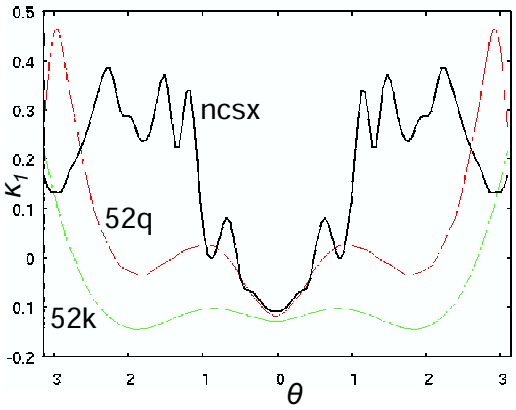

FIG. 7: (Color online) Profiles of $\kappa_1(\theta)$ for the 3 configurations of Fig. 6.

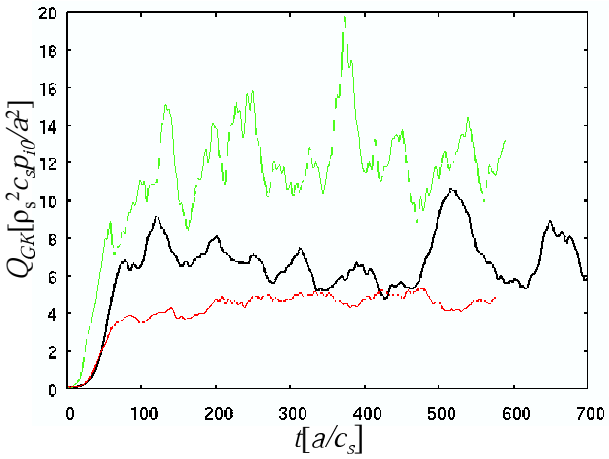

FIG. 8: (Color online) Comparison of heat flux Q_{GK} versus time for the 3 configurations of Fig. 6.

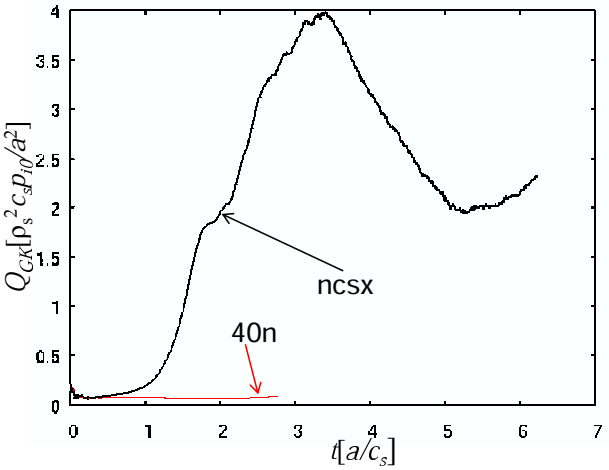

FIG. 9: (Color online) Heat flux Q_{GK} versus time for NCSX (black) and QA_40n for ETG turbulence.